

Switched Reluctance Linear Motor Force Ripple Suppression Based on Fixed Frequency Implicit Generalized Predictive Self-Correction Controller

Jinfu Liu, Hao Chen, *Senior Member, IEEE*, Xing Wang, Patrick Wheeler, *Senior Member, IEEE*, Vitor Fernão Pires, *Senior Member, IEEE*, João Martins, *Senior Member, IEEE*, Antonino Musolino, Yassen Gorbounov, Hossein Torkaman, *Senior Member, IEEE*.

Abstract—An implicit generalized predictive self-correction controller (IGPC) is proposed in this paper to suppress the force ripple of switched reluctance linear motors (SRLMs). Due to its good robustness and rolling optimization features, the dynamic matrix controller (DMC), a kind of multi-step model predictive controller, is considered an effective method to suppress the force ripple of SRLMs. However, because DMC uses a fixed predictive model, it has high requirements for the accuracy of the predictive model, and the non-linear SRLMs make it difficult to adapt to different loads. To ease this problem, the IGPC proposed in this paper adopts a more flexible predictive model and improves the generalized predictive controller (GPC) to avoid solving the Diophantine equation online, which can adapt to different loads and reduce the system's burden. Besides, the proposed IGPC reduces the computational burden during matrix operations compared to DMC. In the simulation and experimental test based on a 100W 6/4 double-sided SRLM (DSRLM), the proposed IGPC is compared with DMC, and the force distribution function (fdf) adopts the current hysteresis, the results show that the proposed IGPC a better force ripple suppressing performance and has better load capacity compared with DMC.

Index Terms—Switched reluctance linear motor, Predictive control, Generalized predictive control, Self-correction controller Force ripple suppression.

I. INTRODUCTION

Switched reluctance motors are widely used in many industrial applications because of their sturdy construction, large starting torque, and low manufacturing cost[1-4]. However, the torque ripple, caused by the doubly salient structure and non-linear magnetization characteristics, limits

This work was supported by National Natural Science Foundation of China under Grant 51977209 and Cooperation and Exchange Program between NSFC and RS under Grant 52211530083

Jinfu Liu is with the School of Electrical and Power Engineering, China University of Mining and Technology, Xuzhou 221116, China (e-mail: liujinfu99@cumt.edu.cn).

Hao Chen is with the School of Electrical Engineering, China University of Mining and Technology, Xuzhou 221116, China, Xinjiang Institute of Engineering, Urumqi 830000, Xinjiang, China, the International Joint Research Center of Central and Eastern European Countries on New Energy Electric Vehicle Technology and Equipment, Xuzhou 221008, China, the International Cooperation Joint Laboratory of New Energy Power Generation and Electric Vehicles of Jiangsu Province Colleges and Universities, Xuzhou 221008, China, and also with the Xuzhou Key Laboratory of New Energy Electric Vehicle Technology and Equipment, Xuzhou 221008, China (e-mail: hchen@cumt.edu.cn)

Xing Wang is with the International Joint Research Center of Central and Eastern European Countries on New Energy Electric Vehicle Technology and Equipment, Xuzhou 221008, China, the International Cooperation Joint Laboratory of New Energy Power Generation and Electric Vehicles of Jiangsu Province Colleges and Universities, Xuzhou 221008, China, and with the Xuzhou Key Laboratory of New Energy Electric Vehicle Technology and

the development and applications of SRMs[1, 5]. To reduce the torque ripple and improve the performance of SRMs, many control methods are proposed, including phase current control[6], pulse-width modulation (PWM) regulation[7], or directly controlling the converter states[1].

Shaping profiles of phase currents is a widely accepted method to reduce the torque ripple[8], such as the torque sharing function (TSF)[9]. TSF is an effective algorithm to suppress the force ripple in the commutation region. In practical applications, TSF control can be divided into two categories. One is the conversion of the reference torque obtained from the torque distribution function to the reference current[10, 11]. The other type is to directly output the reference torque obtained from the torque distribution function and perform instantaneous torque control[12]. Compared with torque, current detection is more accurate, and the control of current is more conducive to improving other performance of the motor, so the former TSF type is more often used. The system generates reference currents through the torque-sharing function and then simply needs to allow the actual current or torque to follow the reference value, then the torque ripple can be reduced[11, 13]. However, due to the nonlinearity of SRMs and influenced by mutual inductance and saturation, it is difficult to build an accurate analytical model to make the current track the reference. Therefore, classical control linear algorithms such as PI or fuzzy control are difficult to adapt to different motor operating conditions. To handle this problem, a method to reduce the current tracking error has been proposed in the literature[8], in which the value of the reference current is

Equipment, Xuzhou 221008, China (e-mail: 3512@cumt.edu.cn).

Patrick Wheeler is with Power Electronics, Machines and Control Group, The University of Nottingham, Nottingham, UK, (e-mail: Pat.Wheeler@nottingham.ac.uk).

Vitor Fernão Pires is with the Setúbal School of Technology, Polytechnic Institute of Setúbal, 2914-508 Setúbal, Portugal, and also with the Instituto de Engenharia de Sistemas e Computadores, Investigação e Desenvolvimento em Lisboa (INESC-ID), 1049-001 Lisbon, Portugal (e-mail: vitor.pires@estsetubal.ips.pt).

Joao F. A. Martins is with the Department of Electrical Engineering, Faculty of Sciences and Technology, NOVA University of Lisbon, 2829-517 Caparica, Portugal (e-mail: jf.martins@fct.unl.pt).

Antonino Musolino is with the Department of Energy, System, Territory and Construction Engineering (DESTEC), University of Pisa, 56122 Pisa, Italy (e-mail: antonino.musolino@unipi.it).

Yassen Gorbounov is with the Faculty of Automation, University of Mining and Geology “St. Ivan Rilsky” (e-mail: y.gorbounov@mgu.bg).

Hossein Torkaman is with the Faculty of Electrical Engineering, Shahid Beheshti University, Tehran 19839 69411, Iran (e-mail: h_torkaman@sbu.ac.ir).

obtained by off-line calculation according to the reference torque and optimized on this basis. In the literature [8], the current hysteresis loop control is adopted to control the current. Hysteresis loop control is a widely used control method for SRMs, and current hysteresis control is the most widely used in current control due to its simplicity, fast dynamic response, and motor model independence[14]. In addition, torque hysteresis control is also a widely accepted method in direct instantaneous torque control (DITC)[15, 16]. However, the variable chopping frequency is the main drawback of hysteresis loop control, which leads to torque ripple and increases the cost of the digital controller [2, 14, 17]. Some researchers proposed intelligent control algorithms like neural networks[5]. The main disadvantage of these methods is that large amounts of data are required to train the model offline to ensure the accuracy of the model.

Model predictive control (MPC) originates from the practical application of industrial and is increasingly used in industrial process control. Because of its multi-step prediction, rolling optimization, and feedback correction control strategies, MPC controllers have the advantages of good control effect, high robustness, and low requirements for model accuracy. On the other hand, the development of the microprocessor makes it possible to handle larger matrix dimensions, which will further improve the effect of MPC [18]. Many efforts at current or torque control of SRMs based on MPC have recently been published. Literature [19] proposed a multi-step prediction algorithm for SRMs, based on the prediction of the future state of the system, the value of the next stage of control is calculated through the cost function. [20] proposed a novel MPC algorithm, which reduces the computation burden of the system. Conventional MPC requires multiple iterations and results in fixed coefficient matrix dimensions. Thus, in the case of multi-step prediction, it will increase the burden of the system. Moreover, the fixed predictive model limits the dynamic performance of the system. Although rolling online optimization is possible, the predictive model needs to be rebuilt when the control target changes. Generalized predictive control (GPC) is based on the CARIMA model and adopts a long-time optimization performance index, which is more robust and has a wide range of applications[21]. Different from the conventional MPC, the GPC control algorithm does not need a fixed model, instead, the previous input and output information are used to estimate the model parameters online and to correct the control law, which is named the enlightened control algorithm. For this reason, by setting the control horizon and prediction horizon of the system, the dimension of the coefficient matrix during the calculation process can be set manually, which makes it possible to reduce the computational burden of the system. GPC does not consider the error prediction model and gives the predicted value by online correction instead, which has the feature of adaptive control. In this way, even if the target changes, the GPC controller can also build up a predictive model during the operation. Besides, in the SRM-driven algorithm, GPC provides a fixed switching frequency because of its modulation stage[22], which can overcome the disadvantage of the hysteresis loop control. In

addition, the rolling optimization of MPC is retained so that GPC inherits many of the advantages of MPC. During the operation of GPC, the Diophantine equation is required to be solved multiple times, which increases the burden of the system. Compared with a normal GPC controller, the implicit generalized predictive self-correction controller (IGPC) avoids the drawback that GPC requires multiple solutions of the Diophantine equation for multi-step prediction, which reduces the burden of the system. Compared with MPC based on dynamic matrix control (DMC) indicated in [19], IGPC does not need the accuracy parameters of motors, and the same as the traditional GPC, IGPC can also set the dimension of the coefficient matrix manually to further reduce the calculation burden.

In the scene requiring linear motion, rotary motors like SRMs generally need additional crank linkage, which causes mechanical wear and tear and reduces system efficiency. For this reason, the linear motor is used in many industrial applications[23-25]. Since the switched reluctance linear motors (SRLM) have a similar structure to SRMs, they inherit many advantages of SRMs. However, since the stator windings of SRLM are not periodically arranged, they are affected by the longitudinal edge-end effect, which makes it difficult to establish an accurate model and increases the force ripple[26]. The IGPC controller proposed in this paper does not consider the specific model of the motor, which is suited for SRLM. As a type of SRLM, the double-sided switched reluctance linear motor (DSRLM) has a simple structure, and its double-sided structure can effectively eliminate the normal pulling force, thereby reducing the wear of the linear motor, and having high application value. For this reason, a 6/4 structure 100W DSRLM is used as the prototype in this paper.

In this paper, the basic principles and modeling of IGPC are presented in Chapter II, the determination of initial values of IGPC is presented in Chapter III, the determination of parameters of IGPC is indicated in Chapter IV, the quantitative comparison of the burden on the system between IGPC and DMC is indicated in Chapter V, Chapter VI focuses on the simulation results of the motor, and Chapter VII analyzes the experimental verification results.

II. THE MATHEMATICAL DERIVATION

A. Establishment of normal generalized predictive control model.

To establish a GPC controller, first consider the following CARIMA equation[27]:

$$A(z^{-1})y(t) = B(z^{-1})u(t-1) + C(z^{-1})\frac{\xi}{\Delta} \quad (1)$$

Where the last term is disturbances, z^{-1} is back-shift operator, $\Delta=1-z^{-1}$, which is called differential operator. If $\xi(t)$ is white noise, then the polynomial $C(z^{-1})$ can be assumed as $C(z^{-1})=1$. In equation (1), $A(z^{-1})$ and $B(z^{-1})$ can be expressed as:

$$A(z^{-1}) = 1 + a_1 z^{-1} + \dots + a_{n_a} z^{-n_a}$$

$$B(z^{-1}) = b_0 + b_1 z^{-1} + \dots + b_{n_b} z^{-n_b}$$

To obtain the predictive value $y(k+j|k)$, the following Diophantine equation should be solved:

$$1 = E_j(z^{-1})A(z^{-1})\Delta + z^{-j}F_j(z^{-1}) \quad (2)$$

Where $E_j(z^{-1})$ and $F_j(z^{-1})$ can be expressed as:

$$E_j(z^{-1}) = e_{j,0} + e_{j,1}z^{-1} + \dots + e_{j,j-1}z^{-(j-1)}$$

$$F_j(z^{-1}) = f_{j,0} + f_{j,1}z^{-1} + \dots + f_{j,n_a}z^{-n_a}$$

The degree of $E_j(z^{-1})$ is $j-1$ so that all noise components are in the future. Then the optimum prediction of y derived from (1) and (2) can be expressed as:

$$\hat{y}(k+j|k) = \tilde{G}_j(z^{-1})\Delta u(k+j-1) + F_j(z^{-1})y(k) \quad (3)$$

Define:

$$\tilde{G}_j(z^{-1}) = E_j(z^{-1})B(z^{-1}) = G_j(z^{-1}) + z^{-(j-1)}H_j(z^{-1}) \quad (4)$$

In this way, (3) can be divided into two parts, which are the past and future. The equation (3) can be deduced as:

$$y(k+j|k) = G_j\Delta u(k+j-1|k) + H_j(z^{-1})\Delta u(k) + F_j(z^{-1})y(k) \quad (5)$$

In (5), $H_j(z^{-1})\Delta u(k) + F_j(z^{-1})y(k)$ is the response of the past values of input and output, which is called free response. And $G_j\Delta u(k+j-1|k)$ is consists of the response to future values of actuating variables, which is called forced response. According to (5), for n -step prediction, the matrix form of the equation can be expressed as:

$$\hat{\mathbf{Y}} = \mathbf{G}\tilde{\mathbf{u}} + \mathbf{f} \quad (6)$$

Where, $\tilde{\mathbf{u}} = [\Delta u(k), \Delta u(k+1), \dots, \Delta u(k+n-1)]^T$, $\mathbf{f} = [f(k+1), f(k+2), \dots, f(k+n)]^T$, $\hat{\mathbf{Y}} = [\hat{y}(k+1), \hat{y}(k+2), \dots, \hat{y}(k+n)]$, in (6), for reducing the matrix dimension to reduce the burden of the system, the control horizon m is introduced in this paper. When $j > m$, set $\Delta u(k+j-1|k) = 0$, then the dimensionality of \mathbf{G} is $n \times m$, n is the predictive horizon, which reduces the calculation burden of the system. When $m=1$, $(\mathbf{G}^T \mathbf{G} + \lambda \mathbf{I})$ will be a scalar quantity. It can be proved that the first j terms of $G_j(z^{-1})$ are independent of j . And then define:

$$\mathbf{G} = \begin{bmatrix} g_0 & \cdots & \mathbf{0} \\ \vdots & \ddots & \vdots \\ g_{n-1} & \cdots & g_0 \end{bmatrix}$$

From (5), the individual components of the vector \mathbf{f} are denoted as:

$$f(k+n) = H_n(z^{-1})\Delta u(k) + F_n(z^{-1})y(k) \quad (7)$$

The matrix form of (9) can be expressed as:

$$\mathbf{f} = \mathbf{H}\Delta \mathbf{u}(k) + \mathbf{F}y(k) \quad (8)$$

Same as DMC in [19], GPC also uses a cost function for rolling optimization, which both the following performance of the system and the system control volume kept from fluctuating drastically are taken into account:

$$J = (\hat{\mathbf{Y}} - \mathbf{w})^T (\hat{\mathbf{Y}} - \mathbf{w}) + \lambda \tilde{\mathbf{u}}^T \tilde{\mathbf{u}} \quad (9)$$

Where, $\mathbf{w} = [w(k+1), w(k+2), \dots, w(k+n)]^T$ is the reference track of the system, λ is weighting factor. In this way, the controlled quantity follows the reference trajectory to

gradually approach the reference value, thus reducing system oscillations. The reference track is generated by:

$$w(k+j) = \alpha^j y(k) + (1-\alpha^j)y_r \quad (10)$$

Where, α is the softening factor, $0 < \alpha < 1$. According to (6), (9) can be written as:

$$J = (\mathbf{G}\tilde{\mathbf{u}} + \mathbf{f} - \mathbf{w})^T (\mathbf{G}\tilde{\mathbf{u}} + \mathbf{f} - \mathbf{w}) + \lambda \tilde{\mathbf{u}}^T \tilde{\mathbf{u}} \quad (11)$$

The future control variable $u(k+1)$ that minimizes J will be chosen to determine the input of the system. The minimum of equation (11) is determined by setting the derivative of J equal to zero, solving the equation, then $\tilde{\mathbf{u}}$ can be obtained:

$$\tilde{\mathbf{u}} = (\mathbf{G}^T \mathbf{G} + \lambda \mathbf{I})^{-1} \cdot \mathbf{G}^T (\mathbf{w} - \mathbf{f}) \quad (12)$$

To reduce the burden of the system, considering only the first element of $\tilde{\mathbf{u}}$ is used, then the optimized control variable $u(k)$ can be obtained by:

$$u(k) = u(k-1) + \mathbf{d}^T (\mathbf{w} - \mathbf{f}) \quad (13)$$

Here \mathbf{d}^T is the first row of $(\mathbf{G}^T \mathbf{G} + \lambda \mathbf{I})^{-1} \cdot \mathbf{G}^T$. According to (12) and (13), the optimal control variables can be obtained by solving for \mathbf{G} and \mathbf{f} . In the conventional GPC, the value of \mathbf{G} and \mathbf{f} is calculated by solving the Diophantine equation many times. However, the process of solving Diophantine requires a lot of arithmetic, which increases the burden of the system. The IGPC proposed in this paper avoids solving the Diophantine equation to obtain \mathbf{G} and \mathbf{f} online. Besides, compared with DMC, IGPC reduces the computational dimension of the matrix. Next, the process of calculating free response \mathbf{f} and forced response \mathbf{G} by IGPC will be introduced.

B. IGPC method for solving free response and forced response

1) The calculation of the forced response.

To avoid solving the Diophantine equation, according to equation (6),

$$y(k+1) = g_0 \Delta u(k) + f(k+1) + E_1 \xi(k+1)$$

$$y(k+2) = g_1 \Delta u(k) + g_0 \Delta u(k+1) + f(k+2) + E_2 \xi(k+2)$$

⋮

$$y(k+n) = g_{n-1} \Delta u(k) + \dots + g_0 \Delta u(k+n-1) + f(k+n) + E_n \xi(k+n) \quad (14)$$

It can be noticed from (14) that, all the elements of \mathbf{G} are included in the last equation $y(k+n)$. Therefore, it is only to identify parameters of $y(k+n)$, the matrix \mathbf{G} can be solved. The least squares method is used to identify the parameters of (14), which requires $E_n \xi(k+n)$ to be white noise. However, generally, $E_n \xi(k+n)$ is not white noise. But the deviation between the predictive value $\hat{y}(k|k-n)$ and the actual value $y(k)$ can be regarded as white noise $\varepsilon(k)$, which is:

$$y(k) - \hat{y}(k|k-n) = \varepsilon(k) \quad (15)$$

Define:

$$\mathbf{X}(k) = [\Delta u(k), \Delta u(k+1), \dots, \Delta u(k+n-1), 1]$$

$$\boldsymbol{\theta}(k) = [g_{n-1}, g_{n-2}, \dots, g_0, f(k+n)]^T$$

In connection with (15), the last equation of (14) can be expressed as:

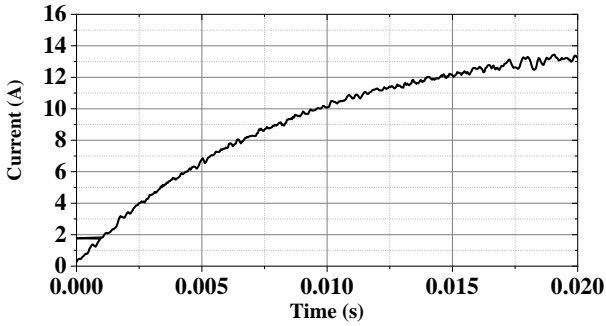


Fig. 2. Current step response waveform at starting position.

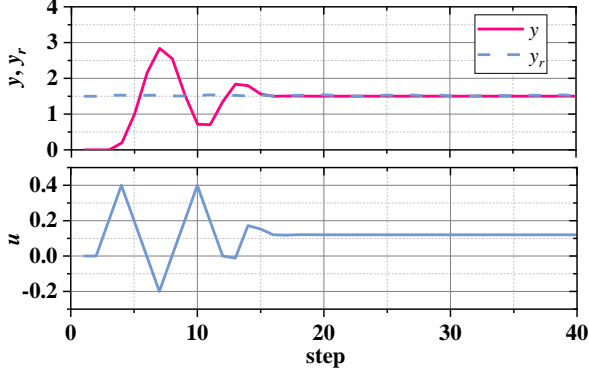


Fig. 3. System input u , output y , and reference y_r at 0mm position under step response.

The parameter of equation (1) at the starting position of the mover $A(z^{-1})$ and $B(z^{-1})$ should be determined first. The least squares estimation similar to (17) is adopted, and the parameter can be defined as:

$$\theta_1(k) = [a_1, \dots, a_{n_a}, b_0, \dots, b_{n_b}]^T$$

$$\varphi(k) = [-\Delta y(k-1), \dots, -\Delta y(k-n_a), \Delta u(k-1), \dots, \Delta u(k-n_b-1)]^T$$

The least-square estimation is expressed as:

$$\begin{aligned} \hat{\theta}_1(k) &= \theta_1(k-1) + \mathbf{K}_1(k) [\Delta y(k) - \varphi(k)^T \theta_1(k-1)] \\ \mathbf{K}_1(k) &= \mathbf{P}_1(k-1) \varphi(k) [\varphi(k)^T \mathbf{P}_1(k-1) \varphi(k) + \mu]^{-1} \end{aligned} \quad (22)$$

$$\mathbf{P}_1(k) = \frac{1}{\mu} [\mathbf{I} - \mathbf{K}_1(k) \varphi(k)^T] \mathbf{P}_1(k-1)$$

In (22), $\hat{\theta}_1(-1) = 0$, $\mathbf{P}_1(-1) = \gamma^2 \mathbf{I}$, γ is a large enough positive number. By equation (22), the $A(z^{-1})$ and $B(z^{-1})$ at the starting position can be determined. Assume that without any filter, $C(z^{-1}) = 1$. Then \mathbf{G} and \mathbf{f} can be calculated by solving the Diophantine equation. However, \mathbf{G} and \mathbf{f} at this time are not the optimal values suitable for DSRLM start-up, which will make the start-up process unstable. Therefore, in this paper, MATLAB is used for further processing. Upon obtaining the value of $A(z^{-1})$ and $B(z^{-1})$ through equation (22), the model of equation (1) can be determined and input into MATLAB as the model of DSRLM. The Diophantine equation in Chapter II can then be solved to calculate \mathbf{G} and \mathbf{f} , which can be inputted into the model. Through the iterative calculation of equations (17) and (21), input and output can converge, and \mathbf{G} and \mathbf{f} at this point can be considered the final determined initial values. The change process of input and output is shown in Fig. 3.

Set $m=2$, $n=6$, the results of the calculation are:

$$\mathbf{G}_{init} = \begin{bmatrix} -0.6506 & 0 \\ 0.1522 & -0.6506 \\ 0.2373 & 0.1522 \\ 0.2029 & 0.2373 \\ 0.2144 & 0.2373 \\ 0.6041 & 0.2144 \end{bmatrix}$$

$$\mathbf{f}_{init} = \begin{bmatrix} 2.003 \\ 2.003 \\ 2.003 \\ 2.003 \\ 2.003 \\ 2.003 \end{bmatrix}$$

The mathematical model of the motor at the starting position is thus obtained:

$$\mathbf{Y}_{start} = \mathbf{G}_{init} \mathbf{u}(k) + \mathbf{f}_{init} \quad (23)$$

Among them, the output matrix \mathbf{Y} represents the current, and the input matrix \mathbf{u} represents the duty cycle.

B. IGPC stability determination based on Kleinman controller

Kleinman controller is an effective method to prove the stability of the system[28]. The standard form of the state space model is:

$$\mathbf{x}(k+1) = \mathbf{A}\mathbf{x}(k) + \mathbf{B}\Delta\mathbf{u}(k) \quad (24)$$

Where \mathbf{A} and \mathbf{B} are calculated by parameters of $A(z^{-1})$ and $B(z^{-1})$ of (1), which can be obtained through (25) online [29]:

$$\mathbf{A} = \begin{bmatrix} -\tilde{\alpha}^T & -\alpha_n \\ \mathbf{I}_{n-1} & \mathbf{0} \end{bmatrix}$$

Where,

$$\begin{aligned} \tilde{\alpha}^T &= [\tilde{a}_1, \tilde{a}_2, \dots, \tilde{a}_{n-1}] \\ \tilde{a}_n &= a_n - a_{n-1} \\ \mathbf{B} &= [1, 0, \dots, 0]^T \end{aligned}$$

And \mathbf{x} is the predictive variable, $\mathbf{u}(k)$ is the input, for the system with m -dimensional input and n -dimensional output, the control law is:

$$\Delta u_s(k) = -\gamma \mathbf{B}^T (\mathbf{A}^T)^N \left[\sum_{h=m}^N \mathbf{A}^h \mathbf{B} \gamma^{-1} \mathbf{B}^T (\mathbf{A}^T)^h \right]^{N+1} \mathbf{x}(k) \quad (25)$$

Where $\gamma > 0$, if \mathbf{A} is non-singular, when and only when $N-m \geq n-1$, the control law (25) makes the system expressed as (24) closed-loop stable [30]. It should be noticed that γ , N and m are only parameters of (25), and are not related to the previous expressions, which are literature conventions. If the result of (25) is input into the system, the stability of the system can be guaranteed. Based on this, an assumption can be made that, known that the last input $u(k-1)$ makes the system stable, and the input calculated by (25) $u_1(k) = u(k-1) + \Delta u_s(k)$ is stable, then it is considered that any value between $u(k-1)$ and $u_1(k)$ will make the system stable. From this, for the stability of the system, a constraint to the system's inputs is added:

$$u(k) = \begin{cases} u(k-1) + \Delta u_s(k), & |u_1(k) - u(k-1)| < |\Delta u(k)| \\ u(k-1) + \Delta u(k), & |u_1(k) - u(k-1)| \geq |\Delta u(k)| \end{cases} \quad (26)$$

Where $\Delta u(k)$ is generated by rolling optimization of IGPC

and calculated by (16).

IV. DETERMINATION OF PARAMETERS OF IGPC

A. The parameter determination of IGPC based on DSRLM.

1) Predictive horizon n

To reduce the computational complexity of the system, the values of n and m need to be determined first. The value of n affects the dynamic performance of the system, the increment of n can greatly improve the dynamic performance of the system. However, when it increases beyond a certain range, it does little to improve dynamic performance and will increase the calculation burden. Based on equation (23), we tested different n values, hoping to obtain the minimum n value that can ensure the dynamic performance of the system. To select an appropriate value of n , the reference value of the system is set to a periodic square wave of values 0-2 to observe the system's dynamic performance. The comparison of outputs of different values of n is shown in Fig. 4.

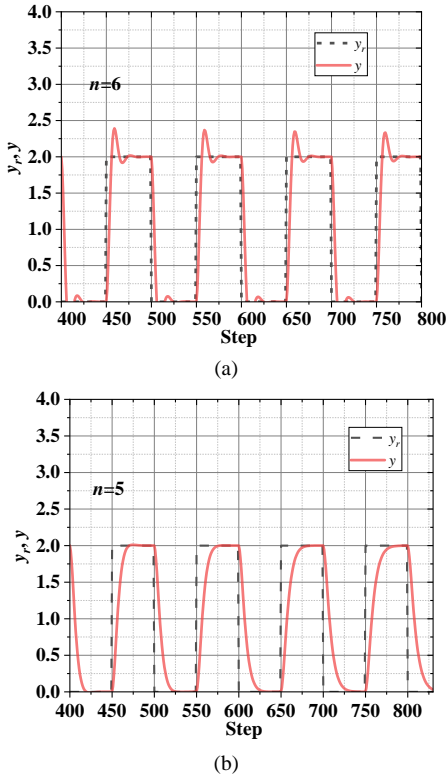


Fig. 4. System outputs of different n .

In Fig. 4, the vertical axis is the current, and the horizontal axis is the number of cycles to execute the IGPC module. Decrement the value of n one by one starting from 7, from the indication of Fig. 4, when the value of n changes from 6 to 5, the dynamic performance is significantly reduced. For this reason, n is set to 6.

2) The control horizon m

The value of m mainly influences the dimension of G . A small value of m can generate a smooth output, which is favorable to system stability. A larger m will increase the speed of the system, which helps to enhance the performance of the

system. However, a too-large m will greatly increase the calculation burden of the system. Generally, m is set to 1~3. Take equation (23) in Chapter III as the model of DSRLM, the impact of parameter m is shown in Fig. 5.

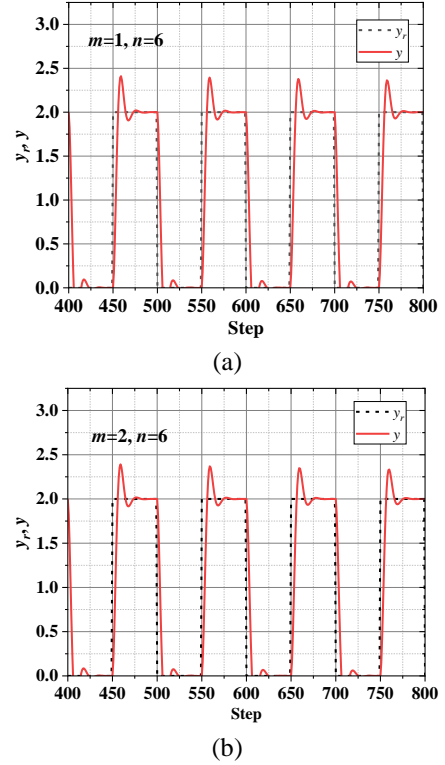


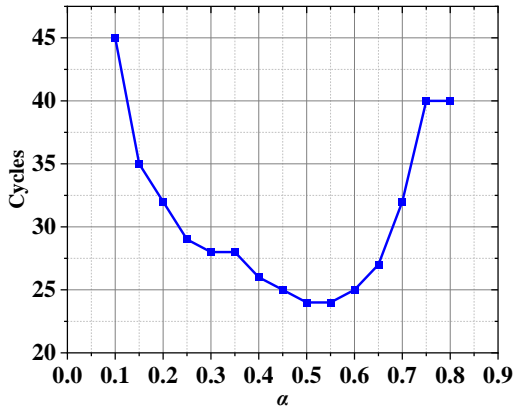
Fig. 5. The dynamic performance under different values of m .

It can be observed that the value of m has little influence on the dynamic performance of the system, which shows that appropriately reducing m to reduce the dimension of matrix G will not significantly reduce the performance of IGPC. When the value of m changes from 1 to 2, the overshoot reduces by about 2%. In this paper, according to convention, and from the perspective of system computing burden, m is set to 2.

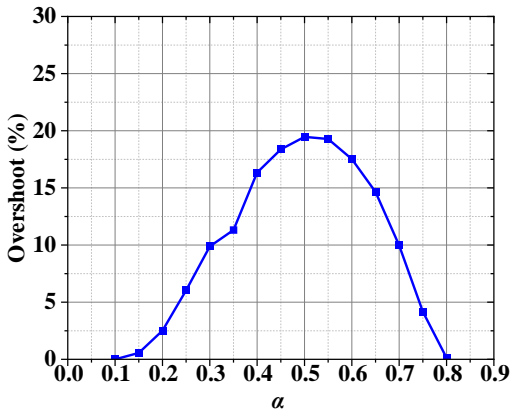
3) Softening factor α

The factor α mainly influence the following rate of the system. If α is small, $w(k)$ will reach the reference value fast, the following performance will be improved. However, the stability of the system will be reduced. When increases α , the quickness of the system will be decreased and the stability of the system will be enhanced on the contrary. The DSRLM model (23) is calculated in MATLAB, set $n=6$, $m=2$, and the dynamic performance under different softening coefficients is obtained.

The dynamic performance of the system under different softening coefficients is shown in Fig. 6. In Fig. 6(a), the vertical axis is the number of cycles required to reach a steady state value, and the horizontal axis is the values of α . Fig. 6(b) indicates the overshoot under different softening coefficients.



(a)



(b)

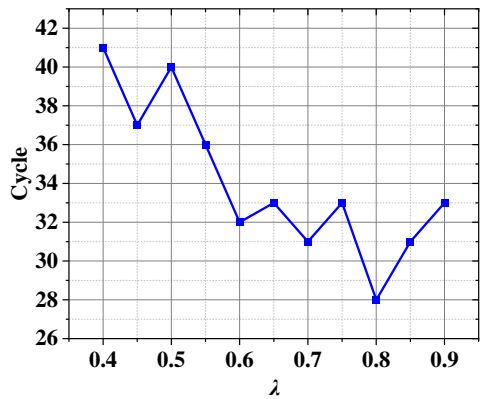
Fig. 6. Dynamic performance of the system under different softening coefficients. (a) Number of cycles to reach steady state value under different α ; (b) Overshoot under different α .

Comprehensive Fig. 6(a) and Fig. 6(b), taking into account the rapidity and stability of the system, the softening coefficient is set to 0.35.

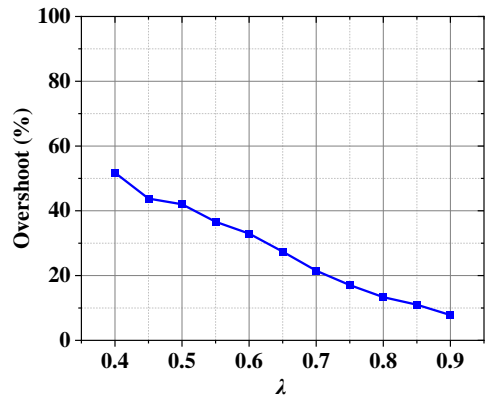
4) Weight coefficient λ

As a weight coefficient, λ mainly affects the inputs of the system, which can reduce the vibration of the input quantity during operation. If the value λ is too small, the stability of the system will be reduced. And if λ is too large, the rapidity of the system will deteriorate. To find the optimal value of λ , take (23) as the model as the motor, under different weight coefficients λ , the adjustment time of the system is as shown in Fig. 7.

It can be seen from Fig. 7 that when λ increases, the system's overshoot decreases and the number of algorithm execution cycles has an overall downward trend until λ is below 0.8. When λ is greater than 0.8, the rapidity of the system becomes worse. Therefore, the weight coefficient λ is set to 0.8 in this paper.



(a)



(b)

Fig. 7. Dynamic performance of the system under different weight coefficients. (a) the number of cycles of IGPC required to enter a stable state; (b) the overshoots.

V. QUANTITATIVE ANALYSIS OF SYSTEM BURDEN

To quantify the operational burden that different control algorithms add to the system, and based on this, determine the sampling period, this chapter counts the number of multiplication and addition operations in the matrix operations of different methods. For traditional GPC and IGPC, the main difference between the proposed IGPC and the traditional GPC in operation is that in terms of solving G and f , IGPC avoids solving the Diophantine equation and only needs to calculate (17) and (21). The process of solving the Diophantine equation is relatively complicated, which greatly increases the computational complexity of the system [27]. Therefore, the IGPC proposed in this paper has a greatly reduced computational complexity compared with the traditional GPC. Therefore, this chapter mainly compares the computational burden between IGPC and DMC.

The following rules are used to quantify the computational burden of statistical systems:

1. When adding two matrices, if the matrix dimension is $m \times n$, $m \times n$ addition operations are required;
2. When multiplying matrices, if the dimensions of the two matrices are $n \times m$ and $m \times w$, the number of multiplication operations required is $n \times m \times w$, and at the same time, the number of addition operations required is $n \times w \times (m-1)$;
3. The inversion operation of an m -dimensional matrix

requires $4m^3/3 - m^2/2 + m/6$ addition operations and $m^3 - m$ multiplication operations.

A. Proposed IGPC compared with DMC

1) Statistics on the number of multiplications and additions in the process of calculating matrix \mathbf{G} in IGPC

According to the computational statistical rules described above, based on equation (17), when the predictive horizon is n and the control horizon is m , the number of multiplication operations N_{mG} and addition operations N_{aG} in the calculation process of \mathbf{G} can be calculated. As the previous indication, $n=6$, $m=2$, then it can be calculated that $N_{mG}=469$, $N_{aG}=406$.

2) Statistics on the number of multiplications and additions in the process of calculating matrix \mathbf{B} in DMC

According to the literature [19], the predictive model is expressed as:

$$\begin{bmatrix} \phi_{k+1|k} \\ \vdots \\ \phi_{k+N|k} \\ \vdots \\ \phi_{k+H_p|k} \end{bmatrix} = \begin{bmatrix} a_k \\ \vdots \\ \prod_{j=1}^N a_{k+j-1} \\ \vdots \\ \prod_{j=1}^{H_p} a_{k+j-1} \end{bmatrix} \cdot \phi_k + \begin{bmatrix} b_k & 0 & \cdots & 0 \\ \vdots & \vdots & \ddots & \vdots \\ b_k \prod_{j=1}^N a_{k+j-1} & b_k \prod_{j=2}^N a_{k+j-1} & \cdots & 0 \\ \vdots & \vdots & \ddots & \vdots \\ b_k \prod_{j=1}^{H_p} a_{k+j} & b_k \prod_{j=2}^{H_p} a_{k+j} & \cdots & b_k a_{k+H_p} \end{bmatrix} \begin{bmatrix} d_k \\ \vdots \\ d_{k+N-1} \\ \vdots \\ d_{k+H_p-1} \end{bmatrix} U_p \quad (27)$$

Where, $a_k = 1 - \frac{T_s \cdot R_p}{L_k}$, $b_k = T_s$, T_s is the sampling time, and L_k

is the phase inductance. ϕ is the flux-linkage, and d_k is the duty cycle. define matrix \mathbf{B} :

$$\mathbf{B} = \begin{bmatrix} b_k & 0 & \cdots & 0 \\ \vdots & \vdots & \ddots & \vdots \\ b_k \prod_{j=1}^N a_{k+j-1} & b_k \prod_{j=2}^N a_{k+j-1} & \cdots & 0 \\ \vdots & \vdots & \ddots & \vdots \\ b_k \prod_{j=1}^{H_p} a_{k+j} & b_k \prod_{j=2}^{H_p} a_{k+j} & \cdots & b_k a_{k+H_p} \end{bmatrix} \quad (28)$$

When the prediction horizon is H_p , the number of multiplication operations N_m in matrix \mathbf{B} is:

$$N_m = \sum_{N=1}^{N=H_p} \sum_{i=1}^{N-1} i \quad (29)$$

Since the calculation of a_k also requires one multiplication operation and one addition operation, the total number of multiplication operations required N_{mt} is:

$$N_{mt} = N_m + H_p - 1 \quad (30)$$

According to the equation (28) and (29), when the predictive horizon is 6, the multiplication operation is 41.

3) Calculation of control variable $u(k)$ of DMC

Since the DMC proposed in [19] is based on the motor balance equation, the dimension of matrix \mathbf{B} is fixed. According to the end of Chapter II, IGPC is not based on fixed equations, so the dimensions of matrix \mathbf{G} are more flexible, just requires the matrix \mathbf{G} to include all g elements. Therefore, for calculating

control variables $u(k)$, the calculation amount of IGPC and DMC is also different.

According to the literature [19], when the prediction step size is 6, the $u(k)$ calculation needs multiplication operations 1567 times and addition operations 1332 times.

4) Calculation of control variable $u(k)$ of IGPC

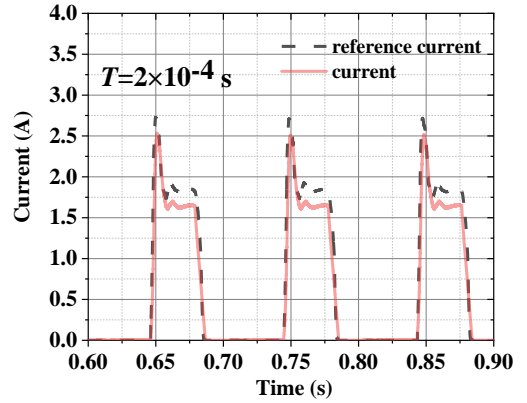
According to equation (13), when set $n=6$, $m=2$, the calculation of $u(k)$ of IGPC needs multiplication operations 81 times and addition operations 62 times.

In general, the comparison of the overall addition and multiplication processes of DMC and IGPC in the operation process is shown in Table I.

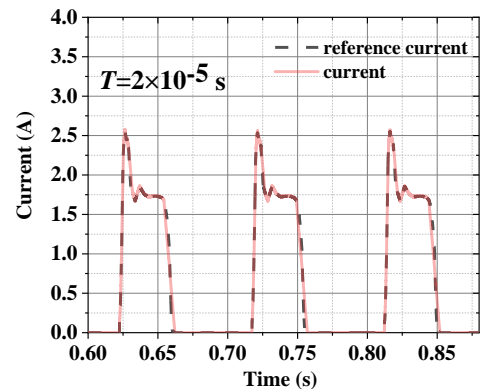
TABLE I
STATISTICS ON THE NUMBER OF MULTIPLICATIONS AND ADDITIONS DURING IGPC AND DMC CALCULATIONS

	IGPC	DMC in [19]
Addition	468	1332
Multiplication	550	1608

It can be observed from Table I that since the dimensions of matrix \mathbf{G} of IGPC are more flexible by setting n and m , the system burden in the calculation process can be effectively reduced. Although literature [19] proposed a method to reduce the computational burden, it still needs to be calculated offline and stored in the LUT, occupying the system's memory.



(a)



(b)

Fig. 8. The influence of the control period.

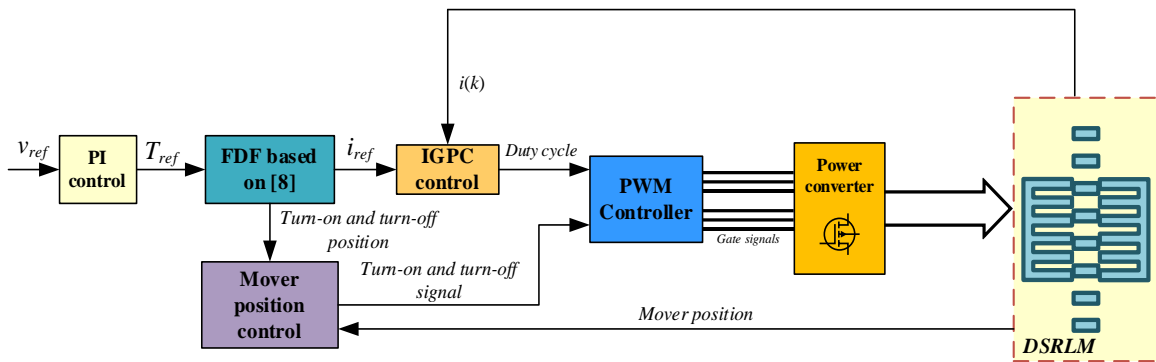


Fig. 9. The structure of the current control system.

B. Controlling period determination

The controlling period T determines the predictive step period and directly impacts the matrix \mathbf{G} . A large value of T contributes to the stability of the system, however, if the selected value is too large, the control performance will be decreased. On the contrary, a too-small value of T will significantly increase the calculation burden of the microprocessor, and there is also a risk that the program cannot be fully executed. In this case, we hope to obtain enough control points in the process of rising and falling of the electromagnetic force, thereby improving the electromagnetic force following ability in this process and reducing the electromagnetic force ripple in the commutation area, but it won't add unnecessary burden to the system. Therefore, we need to calculate the algorithm execution time to determine the control period roughly and adjust it in the experiment to get a better control effect. According to the previous statistics, IGPC needs 468 multiplication operations and 550 addition operations for one cycle, according to the existing equipment in the laboratory, the frequency of RT-LAB is 667MHz, so the total calculation time is 1.527×10^{-5} s at least. The sampling step setting should be larger than the calculation time, which means T should be bigger than 1.527×10^{-5} s. In addition, to improve the following performance of the system, we hope to control at least 50 times during the current rise to the reference value. To ensure this condition, this paper conducts the test at the position with the smallest inductance under static conditions. The current rises fastest under this condition because the motor is stationary, there is no back electromotive force, and the inductance is smallest. The control period is calculated with the goal of controlling 50 times to determine the maximum value of the controlling period. After testing, according to Fig. 2, it takes 1.1×10^{-3} s for the current to rise to the rated load, which means the maximum value of the controlling period is 2.2×10^{-5} s. From this, the controlling period in this paper is set to $T=2 \times 10^{-5}$ s. Fig. 8 indicates the performance under two different control times. In Fig. 8(a), $T=2 \times 10^{-4}$ s, where as in Fig. 8(b), $T=2 \times 10^{-5}$ s. As can be seen in Fig. 8, when the control time of IGPC is set to 2×10^{-4} , the tracking error is much higher than that of 2×10^{-5} . As for the frequency of PI control, we follow the general control system setting convention, which is that the outer loop control

frequency is generally half or 1/4 of the inner loop. In this paper, the velocity loop of the PI controller is used as the outer loop, and the current loop of the IGPC controller is used as the inner loop. So, we set the frequency of the PI controller to 20k, and the control period is 5×10^{-5} s respectively.

VI. SIMULATION RESULTS

A. Establishment of the simulation model

The simulation of the system is achieved by the MATLAB/Simulink. Firstly, the parameters of the prototype DSRLM indicated in Table II are calculated by the finite element (FM) calculation software, and the calculation results are stored in the Simulink look-up table (LUT). The structure of the GPC current control system is shown in Fig. 9. According to the parameters calculated by FM, the operating status of DSRLM is simulated. The PI control module generates reference electromagnetic force according to speed deviation. On this basis, the force distribution function (FDF) module proposed in [8] generates the reference current, which is one of the inputs of the IGPC module. The IGPC module generates a fixed-frequency PWM signal to control the on-off of the switch tube.

TABLE II
MAIN PARAMETERS OF THREE-PHASE 6/4 PROTOTYPE DSRLM

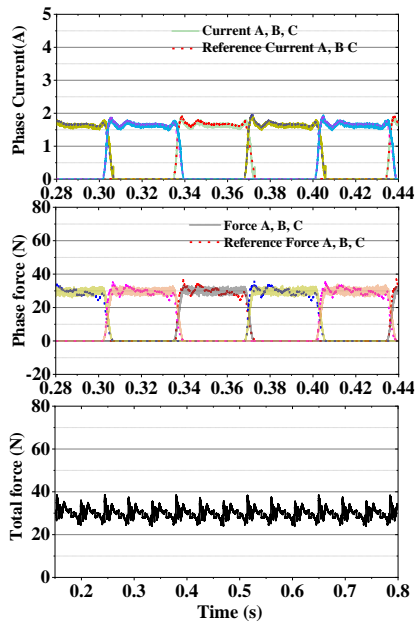
Parameters	Value
Phase number	3
Rated power (W)	100
Maximum power (W)	240
Rated voltage (V)	24
Rated current (A)	4
Base velocity(m/s)	0.4
Stator/mover poles	6/4

B. Comparison with different methods

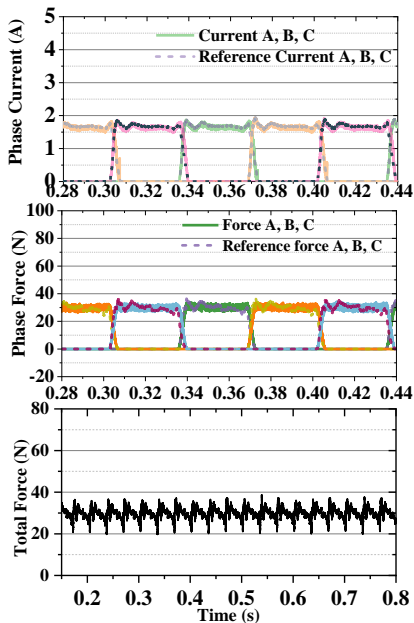
According to the structure of the algorithm indicated in Fig. 10, the simulation model is established in MATLAB /Simulation, the parameters of IGPC that $n=6$, $m=2$, $\alpha=0.35$, $\lambda=0.8$, and the given velocity is set to 0.4m/s. Besides, the simulation models of the FDF proposed in [8] and the DMC control method proposed in [19] are also established in MATLAB /Simulink. The simulation results are shown in Fig.

10.

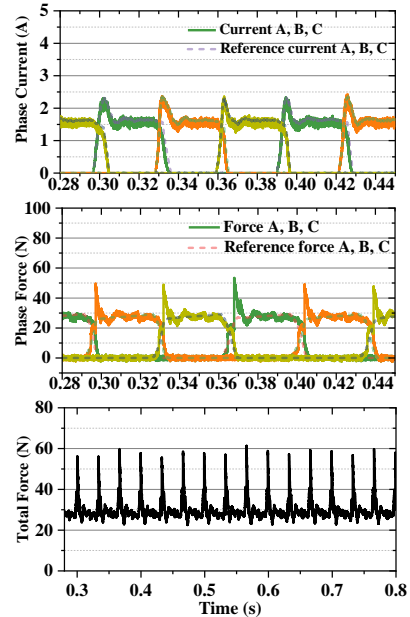
Fig. 10(a) shows the simulation results of the proposed IGPC, Fig. 10(b) depicts the simulation results of the DMC control method proposed in [19], and Fig. 10(c) indicates the FDF control method proposed in the literature [8]. By analyzing Fig. 10(a) and Fig. 10(b), it can be seen that the IGPC algorithm presented in this paper has a similar electromagnetic force ripple suppression effect as the DMC controller introduced in [19]. However, the IGPC algorithm has an advantage in that it does not need the motor parameters to be determined and the dimensions of the coefficient matrix can be artificially defined to reduce the system burden during matrix operations. Compared with the various frequency chopping controllers in [8] shown in Fig. 10(c), due to the fixed frequency chopping method and the rolling optimization process, after adding the IGPC module proposed in this paper, the ability of force ripple suppression is enhanced.



(a)



(b)



(c)

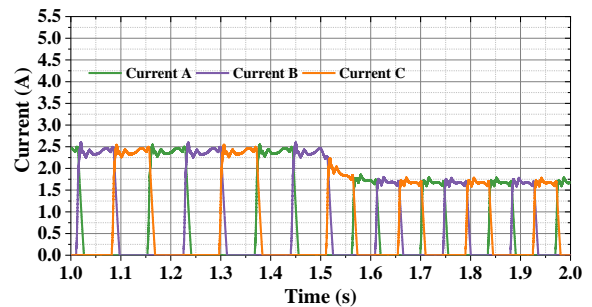
Fig. 10 Simulation results of different control algorithms under 0.4m/s, 30N load. (a)Proposed IGPC. (b) DMC controller proposed in [19]. (c) TSF controller proposed in [8].

C. Dynamic performance test

1) Test of electromagnetic force ripple suppression ability when the load changes suddenly

To verify the feasibility of the system, the dynamic performance of the system was tested by Simulink. Set the load step from 60N to 30N at 1.5s, the simulation results of the current and the total force ripple are shown in Fig. 11(a) and (b).

It can be observed from Fig. 11 that when the load changes, the system can maintain the effect of force ripple suppression. At the same time, the effectiveness and rapidity of the self-correction mechanism of IGPC are verified, which means the system has good stability and anti-interference performance.



(a)

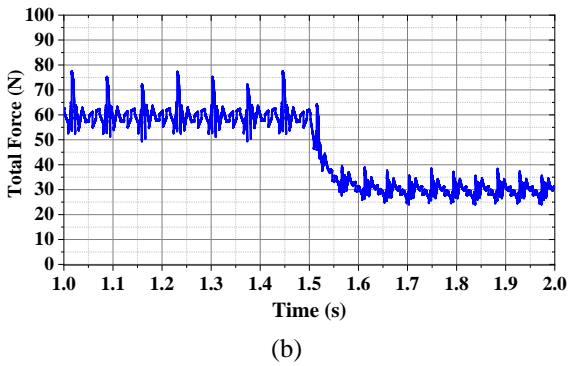


Fig. 11. System dynamic performance simulation results. (a) The phase currents. (b) The total force.

2) System stability test under given velocity step

To verify the stability of the system under the Kleinman controller, the given velocity is set as a step signal, and the simulation results of the mover velocity and phase current are shown in Fig. 12.

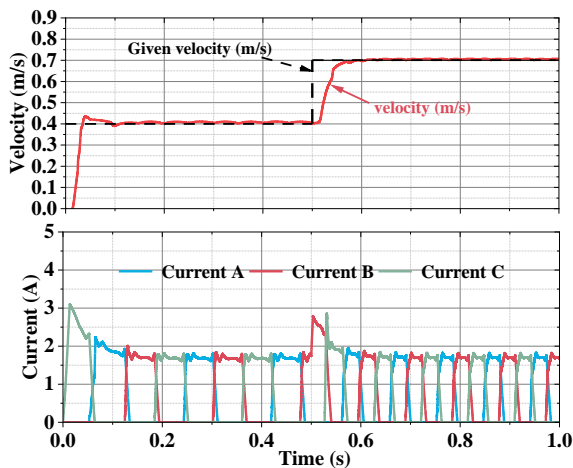


Fig. 12. Stability simulation test of the system at a step-given velocity.

It can be observed from Fig. 12 that when the given velocity is changed from 0.4m/s to 0.7m/s at 0.5s, the moving velocity of the mover can follow the given value well and has good stability. When the speed increases, the current also begins to rise. When the speed stabilizes again since the load remains unchanged, the amplitude of the currents returns to the value before the given velocity steps.

VII. EXPERIMENTAL VERIFICATION

The photo of the experimental platform is shown in Fig. 13. As shown in Fig. 13, the experimental platform consists of the power converter, RT-LAB, isolation circuit, drive circuit, and a prototype DSRLM. The RT-LAB used in this paper, which with 1024Mb SRAM and 667MHz operation frequency, is fully integrated with MATLAB/SIMULINK and MATRIX/System Build. It is easy to build models and has a professional block design for distributed processing. If the model is large and complex, it can easily divide the system model into subsystems, and multiple nodes can be used (That is, the method in which the processors) share a load enabling parallel processing on the target machine and improving the model calculation speed. The

current and voltage detectors of this system use the Hall element sampling method, which has the characteristics of high measurement accuracy, fast response, good linearity, and can achieve electrical isolation detection. LA-100P is used as the current sensor, which has an accuracy of $\pm 0.45\%$ at 25°C , a linearity of $< 0.15\%$, and a response time of less than $1\mu\text{s}$. In this article, A pull-wire encoder is adopted as the position sensor, of which the model is H38S6-1000-3-F-24, total travel is 0-2500mm, the resolution accuracy is 0.0125mm, the repeatability accuracy is 0.01%, and the linear accuracy is 0.05%FS. The RT-LAB analog input board is used to collect current and voltage signals, and the sampling frequency can reach up to 500ks/s. The current and voltage signals are input into the simulation machine after proportional conversion. The electromagnetic force measurement uses a tension sensor with a range of 100N, and the single-phase force measurement uses the look-up table method. The FPGA module embedded in RT-LAB can be well adapted to the online matrix operations of IGPC. A magnetic powder brake is used to simulate the load. The topology of the power converter is three asymmetric half-bridge structures. In this paper, the single-tube chopping method is adopted.

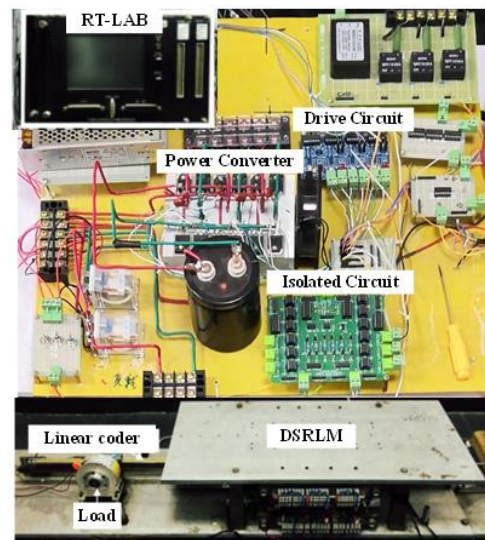


Fig. 13. Actual picture of the experimental platform.

A. Force ripple eliminating ability test

The force ripple-reducing ability of different methods is compared in this chapter. To better measure the magnitude of the force ripple, the force ripple coefficient is introduced, which can be expressed as:

$$F_R = \frac{F_{\max} - F_{\min}}{F_{\text{ave}}} \quad (31)$$

Among them, F_{\max} is the maximum value of the force at the stable operation, F_{\min} is the minimum value of the force at the same operation, and F_{ave} is the average value of the force.

Set the load to 30N and the given speed to 0.4m/s, Chapter IV results were used to set parameters α , λ , n , and m , which are $\alpha=0.35$, $\lambda=0.8$, $n=6$, $m=2$. The force of each phase and the total force are obtained and the frequency analysis results are shown

in Fig. 14. The forces of FDF based on cubic function are shown in Fig. 14(a), the forces of the FDF control algorithm proposed in [8] are shown in Fig. 14(b), the forces of IGPC proposed in this paper are shown in Fig. 14(c), the forces of DMC proposed in [19] are shown in Fig. 14(d).

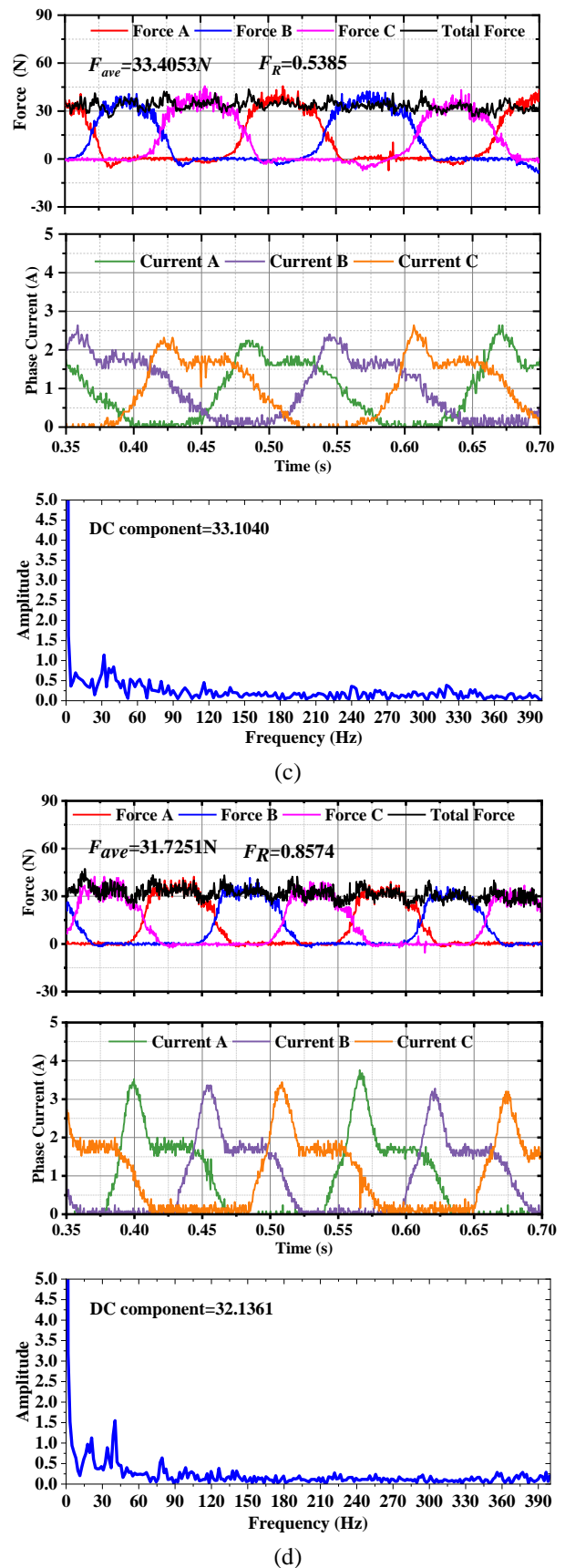
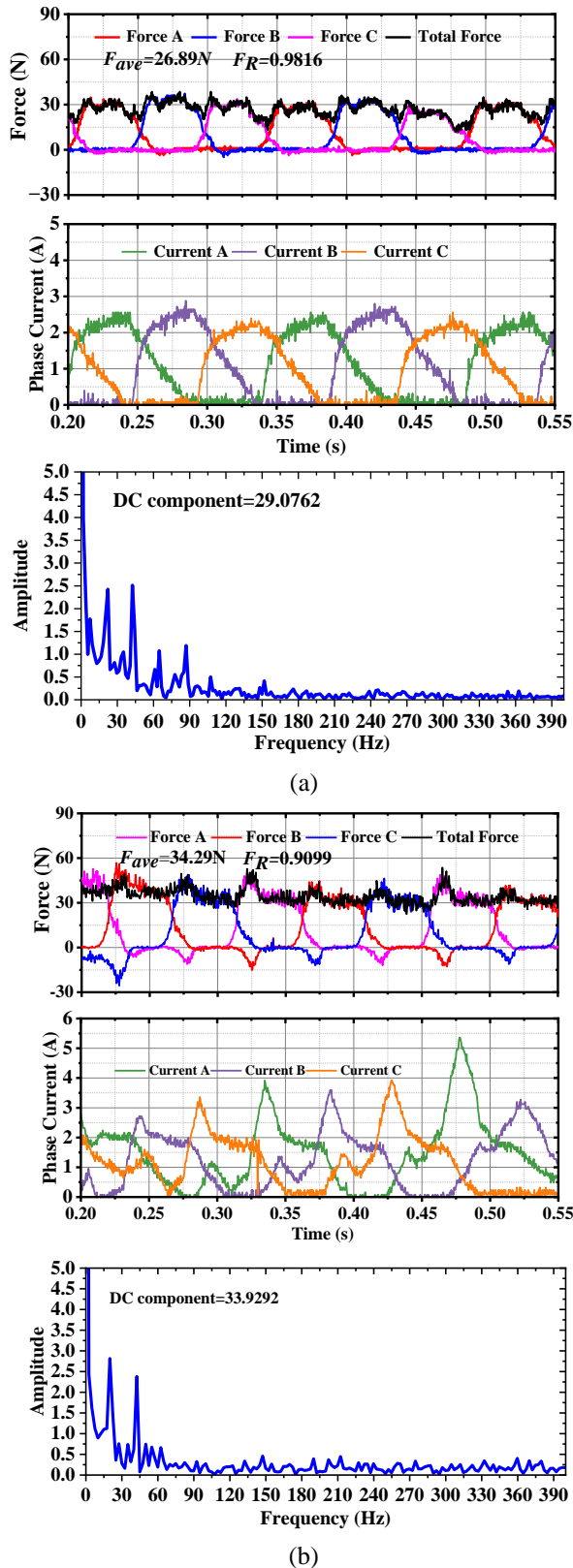
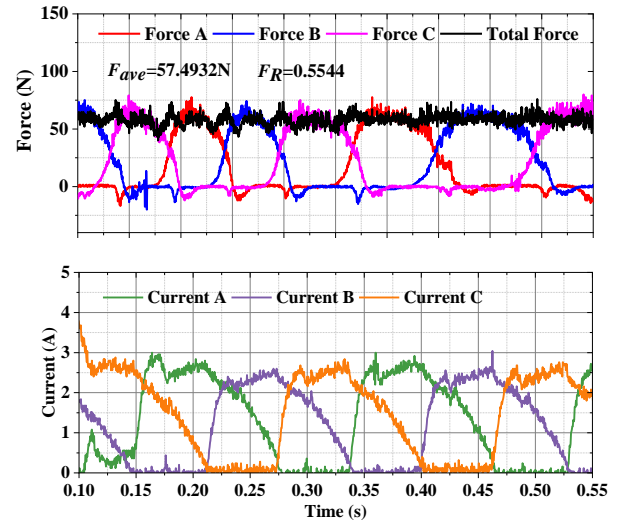


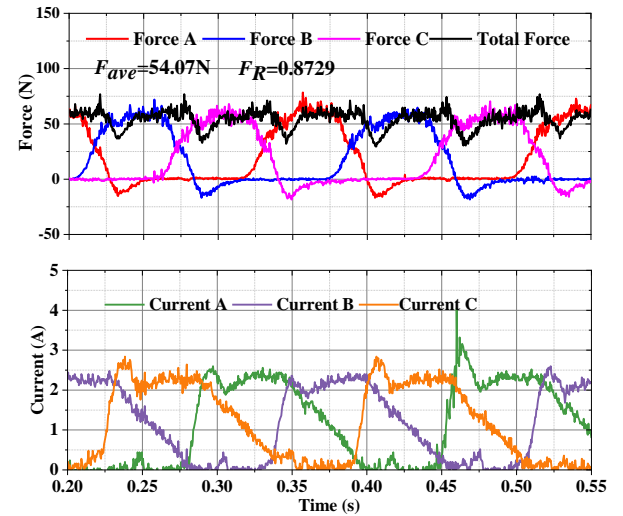
Fig. 14. Experimental results of different control algorithms under 0.4m/s, 30N load. (a) Conversion cubic FDF. (b) FDF proposed in [8]. (c) Proposed IGPC. (d) DMC proposed in [19].

It can be observed that the FDF proposed by [8] can greatly improve the performance of reducing the force ripple compared to Fig. 14(b)-(d) with Fig. 14(a). On this base, because of adopting the fixed chopping frequency and the rolling optimization process, using the same FDF model to generate the reference current, IGPC has better force ripple-eliminating performance according to Fig. 14(b) and Fig. 14(c). Fig. 14(d) indicates the results of DMC proposed by [19], compared with Fig. 14(c), IGPC has a better performance than DMC. This shows that IGPC can still achieve the electromagnetic force ripple suppression of DMC without measuring the parameters of the motor.

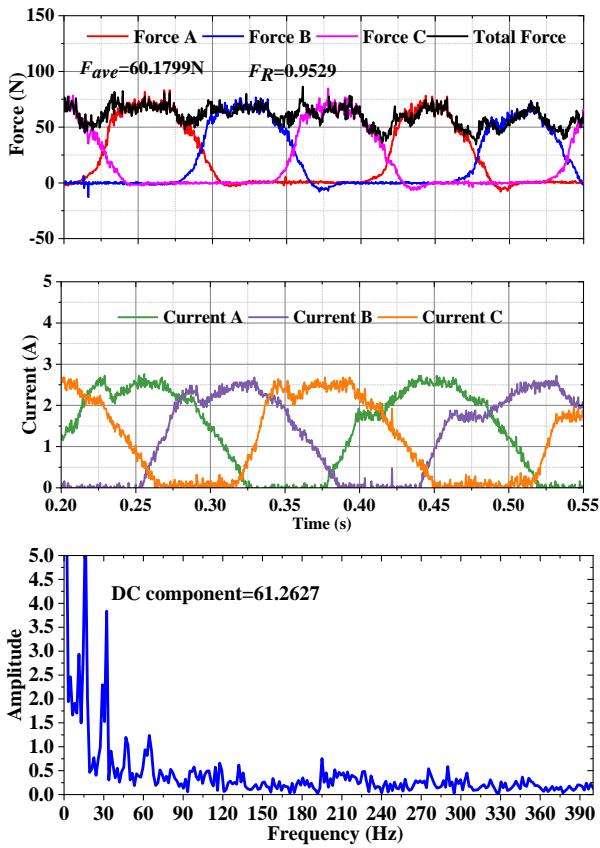
The frequency spectrum of the total force under 30N load is indicated at the bottom of Fig. 14(a)-(d). It can be observed in Fig. 14(a), that in the traditional cubic FDF, the harmonics of the total electromagnetic force are mainly 20Hz, 40Hz, 60Hz, and 80Hz. In Fig. 14(b), in the FDF control method proposed in the literature [8], higher harmonics such as 60Hz and 80Hz are suppressed, but due to the chopping frequency is not fixed, the suppression effect of low-frequency harmonics such as 20Hz and 40Hz is not significant. In Fig. 14(c)-(d), due to the use of predictive control, rolling optimization, and fixed chopping frequency, DMC and IGPC have significantly improved the suppression of harmonics at each frequency, and because of the more flexible predictive model, IGPC has better suppression effect on low-frequency harmonics.



(b)



(c)



(a)

Fig. 15. Experimental results of different control algorithms under 0.4m/s, 60N load. (a) FDF proposed in [8]. (b) Proposed IGPC. (c) DMC proposed in [19].

Then increase the load to 60N, and the results of the total force, phase force, frequency analysis, and phase currents are shown in Fig. 15. According to Fig. 15(a), the performance of force ripple suppression of FDF proposed in [8] is diminished. This is because the current hysteresis loop's ability to control the current is weakened when the load rises and the current rises. It can be observed from Fig. 15(b) that after increasing the load, the IGPC can still maintain good force ripple suppression performance. It can be concluded that the prediction model of IGPC can maintain the control performance at higher currents due to the online self-correction capability and does not depend on the motor parameters, so it is more suitable for SRLM, especially under saturated conditions. As shown in Fig. 15(c), the control effect of DMC is significantly weakened because the motor current increases after increasing the load, and the saturation degree of the stator core changes, so the coefficient matrix with fixed parameters is no longer adapted to the motor operating conditions.

The frequency spectrum of the total force under 60N load is also indicated in Fig. 15. In Fig. 15(a), due to the variable chopping frequency, the FDF proposed in [8] still has significant low-frequency harmonics. In Fig. 15(b), due to the self-correction function of IGPC based on parameter identification, when the motor load changes, the suppression effect of harmonics at each frequency of GPC is better than that of DMC and current hysteresis. It can be seen in Fig. 15(c) that, when the load is 60N, the core saturation degree changes, due to the fixed parameter prediction model, and the suppression effect of DMC on the harmonics of each frequency is significantly reduced.

	FDF in [8]	IGPC	DMC
30N load in simulation	1.0136	0.4875	0.6328
60N in Simulation	1.3142	0.4931	0.6812
30N load in the experiment	0.9099	0.5385	0.8574
60N load in the experiment	0.9529	0.5544	0.8729

The simulation and experimental comparison of electromagnetic force pulsation with different control methods is shown in Table III. It can be observed from Table III that among the three methods, there is a certain deviation between the simulation data and the experimental data. This is due to the deviation between the motor parameters calculated by FEM and the actual motor. Compared with the other two methods, there is not much difference between the simulation data of IGPC and the experimental data. This shows from the side that the impact of motor parameters on IGPC is smaller than that of DMC.

B. Dynamic performance experiments

1) Experiment on electromagnetic force ripple suppression ability when load changes suddenly

Changing the system load abruptly from 60N to 20N, and setting the given speed to 0.6m/s, the dynamic response of the system is shown in Fig. 16. The total force of the proposed

IGPC is shown in Fig. 16(a), and the total force of DMC in [19] is shown in Fig. 16(b). It can be observed that for DMC, the higher the load, the higher the force ripple, which is due to the lack of adaptability of the fixed prediction model of DMC for core saturation. Compared to DMC, IGPC has better dynamic force ripple suppression performance during sudden changes in the load. It can be concluded that the proposed IGPC can better adapt to changes in motor operating conditions due to less dependence on motor parameters, at the same time, the application of the Kleinman controller ensures the stability of the system.

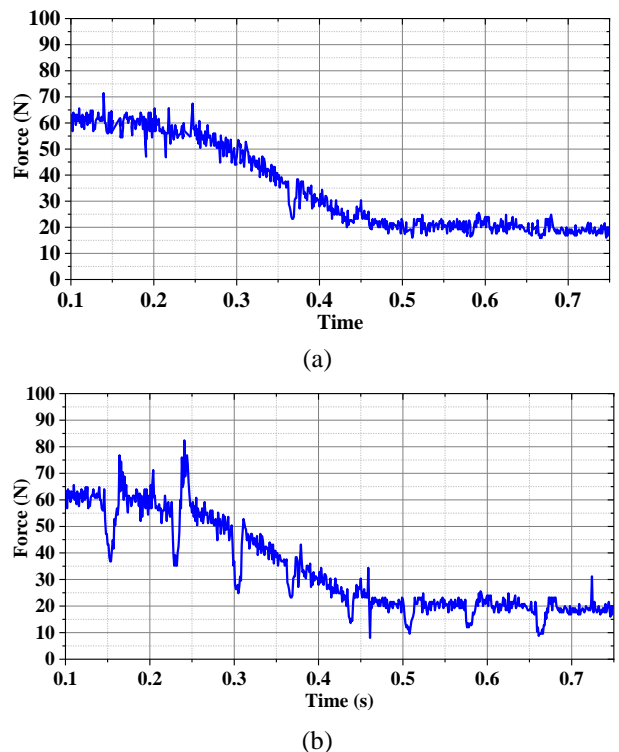


Fig. 16 Dynamic performance experimental results. (a) Proposed IGPC. (b) DMC proposed in [19].

When the load changes, phase currents will also change accordingly, causing the saturation degree of the motor to change, and thus the parameters of the motor will also change. To ensure the dynamic performance of the system, the matrix G needs to be adjusted through the parameter identification function of the algorithm. During this process, the changes in each element of matrix G of IGPC are shown in Fig. 17.

In Fig. 17, it can be seen that, before and after the load mutation point, the elements of G have changed, this means that when the motor parameters change, after the parameter identification process, IGPC adjusts the G matrix and shows good adaptive characteristics. Fig. 18 shows the speed of the mover when the load suddenly changes. It can be observed that when there is a sudden change in load, the velocity of the mover increases temporarily before returning to its original value. This proves the stability of the system.

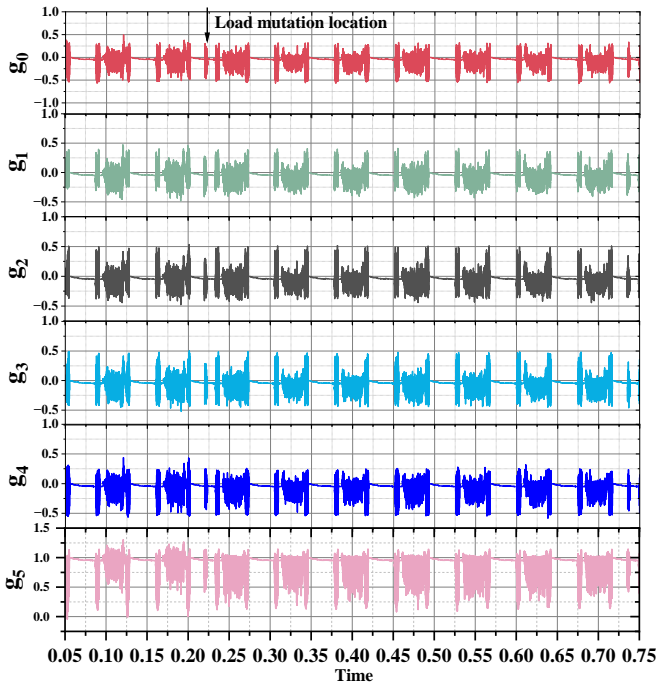


Fig. 17. Each element of matrix G changes when the load changes suddenly.

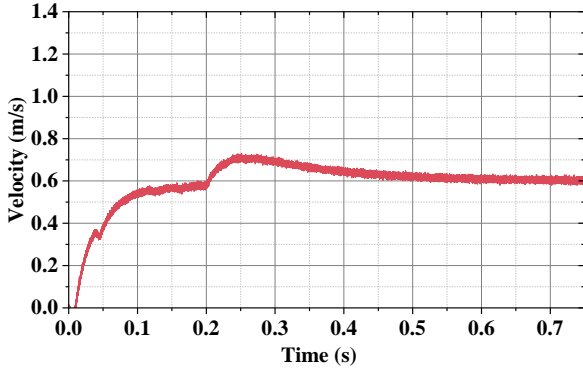
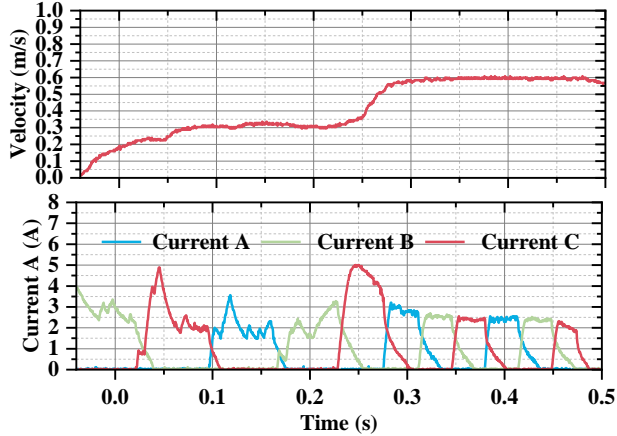
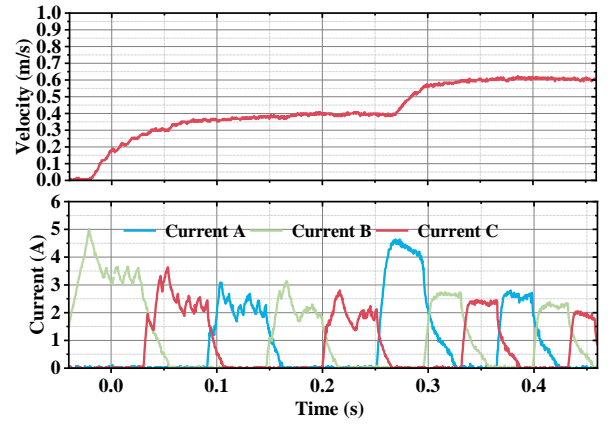


Fig. 18. Speed changes when the load changes suddenly under the IGPC controller.



(a)



(b)

Fig. 19. Experimental results of mover speed and phase current when the given speed is a step signal. (a) Given speed from 0.3m/s to 0.6m/s; (b) Given speed from 0.4m/s to 0.6m/s.

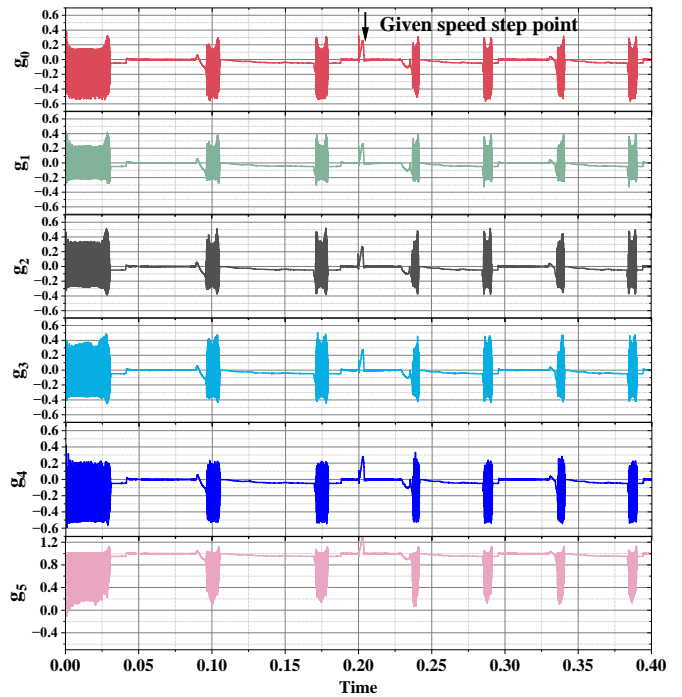


Fig. 20. When the given speed is a step function, the change process of each element of matrix G when the given speed steps from 0.3m/s to 0.6m/s.

2) System stability experiment when the given speed is a step signal

To test the speed regulation capability and stability of the IGPC, the given speed is set as a step signal.

The mover speed and phase currents of the mover are shown in Fig. 19(a)-(b). When the given speed steps from 0.3m/s to 0.6m/s, the mover speed and phase currents are shown in Fig. 19(a), and when the given velocity steps from 0.4m/s to 0.6m/s, the mover speed and phase currents are shown in Fig. 19(b). It can be seen from Fig. 19(a) and Fig. 19(b) that, under different step amplitudes, the mover speed can follow the given value well and has good stability.

In the practice of the given speed step experiment, in the stable state before and after the step point, since only the mover speed changes, the saturation degree remains unchanged before and after the given speed step point. For this reason, the

amplitude of each element of G should also remain unchanged. To verify the stability of G calculation, when the given speed steps from 0.3m/s to 0.6m/s, the change process of each element of matrix G is shown in Fig. 20. It can be observed from Fig. 20 that when the given speed steps, it can be seen that when the speed increases, the change period of each element of G becomes shorter, but the amplitude remains unchanged. At the step point, each element has a small jump. After the speed stabilizes, each element returns to its original value. It can be concluded from this that when the speed changes suddenly, the calculation of G can still ensure a relatively accurate calculation, thus proving the stability of the system from another aspect.

VIII. CONCLUSIONS

A control algorithm based on the implicit generalized predictive self-correction controller (IGPC) is proposed in this paper to suppress the force ripple of a DSRLM. In this paper, a novel force distribution function (FDF) control proposed in [8] and dynamic matrix control (DMC) based on the model predictive control proposed in [19] are compared with the proposed IGPC. Simulation and experimental results show that because of adopting the fixed chopping frequency, IGPC has better performance in reducing the force ripple. Compared with DMC, IGPC can achieve a similar accuracy and doesn't need to measure the parameters of motors, only the online input and output of the system are needed, which has better flexibility. Moreover, IGPC avoids the online iterative process of calculating the coefficient matrix in DMC, while retaining the DMC rolling optimization, it reduces the dependence on motor parameters and the matrix dimension in the process of calculating system input values, thereby reducing the system's computational burden. Compared with the FDF in [8], due to the fixed chopping frequency and rolling optimization, the IGPC has a better electromagnetic force ripple suppression effect of more than 30% improvement than the current hysteresis loop chopping method in [8]. Compared with DMC proposed in [19], IGPC has a better electromagnetic force pulsation suppression effect under heavy load, and changes in motor saturation have less impact on IGPC. However, the calculation process of IGPC is still relatively complex, and the calculation accuracy of the least squares method also needs to be improved. In future research, how to calculate the value of G faster and more accurately is one of the research priorities.

REFERENCES

- [1] N. Yan, X. Cao, and Z. Deng, "Direct Torque Control for Switched Reluctance Motor to Obtain High Torque-Ampere Ratio," *IEEE Transactions on Industrial Electronics*, vol. 66, no. 7, pp. 5144-5152, 2019, doi: 10.1109/tie.2018.2870355.
- [2] L. L. dos Reis, A. A. Coelho, O. M. Almeida, and J. C. Campos, "Modeling and controller performance assessment for a switched reluctance motor drive based on setpoint relay," *ISA Trans*, vol. 48, no. 2, pp. 206-12, Apr 2009, doi: 10.1016/j.isatra.2008.10.012.
- [3] S. K. Sahoo, S. Dasgupta, S. K. Panda, and J.-X. Xu, "A Lyapunov Function-Based Robust Direct Torque Controller for a Switched Reluctance Motor Drive System," *IEEE Transactions on Power Electronics*, vol. 27, no. 2, pp. 555-564, 2012, doi: 10.1109/tpel.2011.2132740.
- [4] S. S. Ahmad and G. Narayanan, "Linearized Modeling of Switched Reluctance Motor for Closed-Loop Current Control," *IEEE Transactions on Industry Applications*, vol. 52, no. 4, pp. 3146-3158, 2016, doi: 10.1109/tia.2016.2550521.
- [5] Z. Lin, D. S. Reay, B. W. Williams, and X. He, "Torque Ripple Reduction in Switched Reluctance Motor Drives Using B-Spline Neural Networks," *IEEE Transactions on Industry Applications*, vol. 42, no. 6, pp. 1445-1453, 2006, doi: 10.1109/tia.2006.882671.
- [6] R. Mikail, I. Husain, Y. Sozer, M. S. Islam, and T. Sebastian, "A Fixed Switching Frequency Predictive Current Control Method for Switched Reluctance Machines," *IEEE Transactions on Industry Applications*, vol. 50, no. 6, pp. 3717-3726, 2014, doi: 10.1109/tia.2014.2322144.
- [7] I. Husain and M. Ehsani, "Torque ripple minimization in switched reluctance motor drives by PWM current control," *IEEE Transactions on Power Electronics*, vol. 11, no. 1, pp. 83-88, 1996, doi: 10.1109/63.484420.
- [8] Z. K. Xia, B. Bilgin, S. Nalakath, and A. Emadi, "A New Torque Sharing Function Method for Switched Reluctance Machines With Lower Current Tracking Error," *Ieee Transactions on Industrial Electronics*, vol. 68, no. 11, pp. 10612-10622, Nov 2021, doi: 10.1109/tie.2020.3037987.
- [9] O. Üstün and M. Önder, "An Improved Torque Sharing Function to Minimize Torque Ripple and Increase Average Torque for Switched Reluctance Motor Drives," *Electric Power Components and Systems*, vol. 48, no. 6-7, pp. 667-681, 2020, doi: 10.1080/15325008.2020.1797939.
- [10] H. Li, B. Bilgin, and A. Emadi, "An Improved Torque Sharing Function for Torque Ripple Reduction in Switched Reluctance Machines," *IEEE Transactions on Power Electronics*, vol. 34, no. 2, pp. 1635-1644, 2019, doi: 10.1109/tpel.2018.2835773.
- [11] J. Ye, B. Bilgin, and A. Emadi, "An Offline Torque Sharing Function for Torque Ripple Reduction in Switched Reluctance Motor Drives," *IEEE Transactions on Energy Conversion*, vol. 30, no. 2, pp. 726-735, 2015, doi: 10.1109/tec.2014.2383991.
- [12] S. Song, R. Hei, R. Ma, and W. Liu, "Model Predictive Control of Switched Reluctance Starter/Generator With Torque Sharing and Compensation," *IEEE Transactions on Transportation Electrification*, vol. 6, no. 4, pp. 1519-1527, 2020, doi: 10.1109/tte.2020.2975908.
- [13] X. D. Xue, K. W. E. Cheng, and S. L. Ho, "Optimization and Evaluation of Torque-Sharing Functions for Torque Ripple Minimization in Switched Reluctance Motor Drives," *IEEE Transactions on Power Electronics*, vol. 24, no. 9, pp. 2076-2090, 2009, doi: 10.1109/tpel.2009.2019581.
- [14] J. Ye, P. Malysz, and A. Emadi, "A Fixed-Switching-Frequency Integral Sliding Mode Current Controller for Switched Reluctance Motor Drives," *IEEE Journal of Emerging and Selected Topics in Power Electronics*, vol. 3, no. 2, pp. 381-394, 2015, doi: 10.1109/jestpe.2014.2357717.
- [15] R. B. Inderka and R. De Doncker, "DITC - Direct instantaneous torque control of switched reluctance drives," *Ieee Transactions on Industry Applications*, vol. 39, no. 4, pp. 1046-1051, Jul-Aug 2003, doi: 10.1109/tia.2003.814578.
- [16] J.-H. Kim and R.-Y. Kim, "Sensorless Direct Torque Control Using the Inductance Inflection Point for a Switched Reluctance Motor," *Ieee Transactions on Industrial Electronics*, vol. 65, no. 12, pp. 9336-9345, Dec 2018, doi: 10.1109/tie.2018.2821632.
- [17] Z. Yu, C. Gan, Y. Chen, and R. Qu, "DC-Biased Sinusoidal Current Excited Switched Reluctance Motor Drives Based on Flux Modulation Principle," *Ieee Transactions on Power Electronics*, vol. 35, no. 10, pp. 10614-10628, Oct. 2020, doi: 10.1109/tpel.2020.2975121.
- [18] S. Vazquez *et al.*, "Model Predictive Control A Review of Its Applications in Power Electronics," *Ieee Industrial Electronics Magazine*, vol. 8, no. 1, pp. 16-31, Mar 2014, doi: 10.1109/mie.2013.2290138.
- [19] X. Li and P. Shamsi, "Model Predictive Current Control of Switched Reluctance Motors With Inductance Auto-Calibration," *IEEE Transactions on Industrial Electronics*, vol. 63, no. 6, pp. 3934-3941, 2016, doi: 10.1109/tie.2015.2497301.
- [20] G. Fang, J. Ye, D. Xiao, Z. Xia, and A. Emadi, "Computational-Efficient Model Predictive Torque Control for Switched Reluctance Machines With Linear-Model-Based Equivalent Transformations," *IEEE Transactions on Industrial Electronics*, vol. 69, no. 6, pp. 5465-5477, 2022, doi: 10.1109/tie.2021.3091918.

- [21] S. Vazquez, C. Montero, C. Bordons, L. G. Franquelo, and Ieee, "Model Predictive Control of a VSI with Long Prediction Horizon," in *20th IEEE International Symposium on Industrial Electronics (ISIE)*, Gdansk, POLAND, Jun 27-30 2011, in Proceedings of the IEEE International Symposium on Industrial Electronics, 2011, pp. 1805-1810, doi: 10.1109/isie.2011.5984431. [Online]. Available: <Go to ISI>://WOS:000297160600285
- [22] D. F. Valencia, R. Tarvirdilu-Asl, C. Garcia, J. Rodriguez, and A. Emadi, "A Review of Predictive Control Techniques for Switched Reluctance Machine Drives. Part I: Fundamentals and Current Control," *IEEE Transactions on Energy Conversion*, vol. 36, no. 2, pp. 1313-1322, 2021, doi: 10.1109/tec.2020.3047983.
- [23] T. Hirayama, S. Yamashita, S. Kawabata, and Ieee, "Design and Analysis of Linear Switched Reluctance Motor with Coreless HTS Excitation Windings for Ropeless Elevator," in *21st International Conference on Electrical Machines and Systems (ICEMS)*, Jeju, SOUTH KOREA, Oct 07-10 2018, in International Conference on Electrical Machines and Systems ICEMS, 2018, pp. 1879-1884. [Online]. Available: <Go to ISI>://WOS:000456286600349. [Online]. Available: <Go to ISI>://WOS:000456286600349
- [24] L. Kolomeitsev *et al.*, "Linear Switched Reluctance Motor as a High Efficiency Propulsion System for Railway Vehicles," in *International Symposium on Power Electronics, Electrical Drives, Automation and Motion*, Ischia, ITALY, Jun 11-13 2008, in International Power Electronics Electrical Drives Automation and Motion SPEEDAM, 2008, pp. 155-+, doi: 10.1109/speedam.2008.4581317. [Online]. Available: <Go to ISI>://WOS:000259920400027
- [25] T. Hirayama, T. Hiraishi, S. Kawabata, and Ieee, "Study on Transfer System with Both Long-Distance Driving and High Positioning Accuracy using Linear Switched Reluctance Motor," in *19th International Conference on Electrical Machines and Systems (ICEMS)*, Chiba, JAPAN, Nov 13-16 2016, in International Conference on Electrical Machines and Systems ICEMS, 2016. [Online]. Available: <Go to ISI>://WOS:000398541900005. [Online]. Available: <Go to ISI>://WOS:000398541900005
- [26] Z. Zhang, N. C. Cheung, K. W. E. Cheng, X. D. Xue, and J. K. Lin, "Longitudinal and Transversal End-Effects Analysis of Linear Switched Reluctance Motor," *Ieee Transactions on Magnetics*, vol. 47, no. 10, pp. 3979-3982, Oct 2011, doi: 10.1109/tmag.2011.2154309.
- [27] A. Linder, R. Kanchan, R. Kennel, and P. Stolze, *Model-Based Predictive Control of Electric Drives*. 2012.
- [28] B. C. Ding and Y. G. Xi, "Stability analysis of generalized predictive control based on Kleinman's controllers," *Science in China Series F-Information Sciences*, vol. 47, no. 4, pp. 458-474, Aug 2004, doi: 10.1360/02yf0239.
- [29] D. W. Clarke and C. Mohtadi, "Properties of Generalized Predictive Control," *IFAC Proceedings Volumes*, vol. 20, no. 5, pp. 65-76, 1987, doi: 10.1016/s1474-6670(17)55480-4.
- [30] D. Kleinman, "Stabilizing a discrete, constant, linear system with application to iterative methods for solving the Riccati equation," *IEEE Transactions on Automatic Control*, vol. 19, no. 3, pp. 252-254, 1974, doi: 10.1109/TAC.1974.1100565.



Jinfu Liu received the B.S. degree in Mechanical and Electrical Engineering, from Northeast Forestry University, Harbin, Heilongjiang, China, in 2017, the M.S. degree from the School of Electrical Engineering, China University of Mining and Technology, Xuzhou, Jiangsu, China, in 2021. He is currently pursuing a Ph.D. degree in electrical engineering at China University of Mining and Technology, Xuzhou, China. His research interests include switched reluctance linear motor control, ocean wave power generation, and electric vehicles.



Hao Chen (Senior Member, IEEE) received his B.S. and Ph.D. degrees in electrical engineering from the Department of Automatic Control, Nanjing University of Aeronautics and Astronautics, Nanjing, China, in 1991 and 1996, respectively. In 1998, he became an Associate Professor with the School of Information and Electrical Engineering, China University of Mining and Technology, Xuzhou, China, where he has been a Professor since 2001. From 2002–2003, he was a Visiting Professor at Kyungshung University, Busan, Korea. Since 2008, he has

also been an Adjunct Professor at the University of Western Australia, Perth, Australia. He is the author of one book and has also authored more than 300 papers. He is a holder of 15 US patents, 23 Australian patents, 1 Danish patent, 7 Canadian patents, 3 South African patents, 10 Russian patents, 79 Chinese invention patents, and 6 Chinese Utility Model patents.



Xing Wang received the B.S. degree from China University of Mining and Technology, Xuzhou Jiangsu, China, in 1996, and M.S. degree from China University of Mining and Technology, Xuzhou Jiangsu, China, in 1999. In 2007, she became an Associate Professor with China University of Mining and Technology, Xuzhou, China. She is a holder of 4 US Patents, 9 Australian Patents, 10 Canadian Patents, 3 Russian Patents, 12 Chinese Invention Patents, 3 Chinese Utility Model Patents, and authored 15 papers.



Patrick Wheeler Patrick W. Wheeler (M'00–SM'13) received the B.Eng. (Hons.) degree from the University of Bristol, Bristol, U.K., in 1990, and the Ph.D. degree in electrical engineering for his work on Matrix Converters from the same university in 1994. In 1993, he moved to the University of Nottingham and worked as a Research Assistant in the Department of Electrical and Electronic Engineering. In 1996, he became a Lecturer in the Power Electronics, Machines and Control Group at the University of Nottingham, Nottingham, U.K. Since January 2008, he has been a Full Professor in the same research group. He has published more than 350 academic publications in leading international conferences and journals., Dr. Wheeler is a Member-at-Large and Distinguished Lecturer of the IEEE Power Electronics Society.



Vitor Fernão Pires (Senior Member, IEEE) received his B.S. degree in electrical engineering from the Instituto Superior of Engineering of Lisbon, Lisbon, Portugal, in 1988, and the M.S. and Ph.D. degrees in electrical and computer engineering from the Technical University of Lisbon, Lisbon, in 1995 and 2000, respectively. Since 1991, he has been a member of the Teaching Staff, the Electrical Engineering Department, Superior Technical School of Setúbal, Polytechnic Institute of Setúbal, Setúbal, Portugal, where he is currently a professor and teaching power electronics and control of power converters. He is also a Researcher with the Instituto de Engenharia de Sistemas e Computadores, Investigação e Desenvolvimento em Lisboa (INESC-ID), Lisbon. His work has resulted in more than 200 publications. His current research interests include the areas of power electronic converters, electrical machines, fault diagnosis and fault-tolerant operation, renewable energy, electrical drives, and power quality.



Joao F. A. Martins (Senior Member, IEEE) graduated in electrical engineering from the Instituto Superior Tecnico (IST), Technical University of Lisbon, Lisbon, Portugal, in 1990. He received the M.Sc. and Ph.D. degrees in electrical engineering from IST, Technical University of Lisbon, in 1996 and 2003, respectively. He is currently with the FCT NOVA, Universidade NOVA de Lisboa, Lisbon, where he is also an Associate Professor with Habilitation, and being currently the Head of the Electrotechnical Engineering and Computers Department. He is also with the Center of Technology and Systems (CTS), UNINOVA, Lisbon, where he coordinates the energy efficiency group and acts as a Communication Officer on the Board of Directors. He has published more than 85 scientific articles in refereed journals and books and more than 180 articles in refereed conference proceedings.



Antonino Musolino received his Ph.D. degree in electrical engineering from the University of Pisa, Pisa, Italy, in 1994. He is currently a Full Professor of electrical machines at the University of Pisa. He has co-authored more than 130 papers published in international journals/conferences. He holds three international patents in the field of magnetorheological devices. His current research activities are focused on linear electromagnetic devices, motor drives for electric traction, and the development of analytical and numerical methods in electromagnetics. Prof. Musolino was involved in the organization of several international conferences, where he has served as the session chairman and an organizer, and as a member of the editorial board.



Yassen Gorbounov received his B.S., M.S., and Ph.D. degrees from the Technical University of Sofia, Republic of Bulgaria, in 2002, 2004, and 2013, respectively. He joined the Faculty of Automation, University of Mining and Geology “St. Ivan Rilsky”, in 2014, and the Department of Informatics, New Bulgarian University, in 2019. In both universities he is presently working as an Associate Professor. His research interests, along with his teaching activities, are in electrical drives and power electronics, digital circuit engineering, robotics, embedded systems, computer architectures, and autonomous vehicles. He is a Senior member of IEEE, took part in more than 15 international projects, and published over 60 scientific works.



Hossein Torkaman (Senior Member, IEEE) is currently an Associate Professor with the Faculty of Electrical Engineering, Shahid Beheshti University, Tehran, Iran. He has published more than 130 technical papers in journal articles and conference proceedings, and four issued patents. He is the author of five books. He was a recipient of different awards and funds from university and companies. He is the Head of the electric machines, power electronics, and motor drives research center laboratory. His main research interests include power electronics, electrical machines, and renewable energies.